Thin-foil expansion into a vacuum with a two-temperature electron distribution function

A. Diaw and P. Mora*

Centre de Physique Théorique, École Polytechnique, Centre National de la Recherche Scientifique, 91128 Palaiseau, France

(Received 5 June 2012; published 7 August 2012)

A kinetic theory of the expansion into a vacuum of a plasma thin foil with initially a hot and a cold Maxwellian electron population is examined with a one-dimensional kinetic code. Whereas hot electrons always lose energy to expanding ions, cold electrons can either gain or lose energy depending on the initial temperature and density ratios and on time. When the cold electrons' density is not too large, they experience initially an adiabatic compression by the electric field associated with the rarefaction wave. The corresponding temperature increase can be as large as a factor of a few tens. Later on, as expected, the cold electrons eventually lose energy to the expansion. When cold electrons are numerically dominant, a rarefaction shock appears during the first phase of the expansion. Hot electrons cool down faster than cold electrons, thus reducing the effective temperature ratio. Furthermore, the amplitude of the rarefaction shock and the dip that it causes on the ion velocity spectrum tend to be smoothed out by the expansion.

DOI: 10.1103/PhysRevE.86.026403 PACS number(s): 52.38.Kd, 52.40.Kh, 52.25.−b, 52.65.Ff

I. INTRODUCTION

The interactions of an ultraintense laser pulse with a solid target can generate ion beams with interesting optical properties [1], high laminarity [2], low divergence [3], and a high energy spectrum [4], which open up many opportunities for their applications in fields such as fast ignition [5], cancer therapy [6], and radiology [7]. Such prospects renew the interest in theoretical studies of plasma expansion into a vacuum [8–13].

In particular, the expansion into a vacuum of a plasma made up of two electron populations, characterized by two electron temperatures, has been the subject of several analytical and numerical works [13–19]. For a semi-infinite plasma, Bezzerides *et al*. [15] demonstrated the occurrence of a rarefaction shock in a plasma composed of two populations of electrons when the ratio of the hot to the cold electron temperatures is larger than $5+\sqrt{24}$. A recent paper [19] extended this work and gave a complete description of the structure of the rarefaction shock and of its influence on the ion acceleration mechanism.

For a thin foil, contrary to the semi-infinite case, one cannot consider that there is an infinite source of particles and energy. In particular the electron hot and cold temperatures become time dependent [13,17], as electrons globally transfer their energy to the ions during the expansion. Moreover, one may expect that each electron population deviates from a Maxwellian distribution function, an effect not usually taken into account in simple fluid models such as those used in Refs. [13,17]. Such kinetic effects in plasma expansion have already been observed in the case of a one-temperature electron distribution function and lead to strong deviations with respect to a Maxwellian distribution function of the same mean energy and to a surprising acceleration of the rarefaction wave [20,21].

In this paper we extend this work by considering kinetic effects in the one-dimensional collisionless expansion into a vacuum of a thin foil with two electron populations. Initially each electron population is described by a Maxwellian distribution function, but the expansion does not preserve the Maxwellian character of each population. We study both the case where the cold electron density is lower than the hot electron density and the more realistic case where the cold electron density is larger than the hot electron density.

II. ELECTRON KINETIC MODEL FOR PLASMA EXPANSION

A. General features

We performed simulations with a nonrelativistic kinetic code describing the collisionless expansion of a one-dimensional plasma slab. The code is fully described in Ref. [20]; it has been validated by detailed comparisons with particle-in-cell simulations. Here we only recall its most peculiar features. The electron dynamics is described by the Vlasov equation, which reads in one-dimensional geometry as

$$\frac{\partial f_e}{\partial t}+v\frac{\partial f_e}{\partial x}+\frac{e}{m_e}\frac{\partial \Phi}{\partial x}\frac{\partial f_e}{\partial v}=0, \tag{1}$$

where $f_e(x,v,t)$ is the electron distribution function, e is the elementary charge, m_e is the electron mass, and $\Phi(x,t)$ is the electrostatic potential. The ions are initially at rest. They are treated as particles and their movement is governed by the equation of motion

$$\frac{dv_i}{dt}=-\frac{Ze}{m_i}\frac{\partial \Phi}{\partial x}, \tag{2}$$

where v_i is the ion velocity, Z is the ion charge number, and m_i is the ion mass. The electrostatic potential Φ satisfies Poisson's equation

$$\frac{\partial^2 \Phi}{\partial x^2}=\frac{e}{\epsilon_0}(n_e-Zn_i), \tag{3}$$

where n_e is the electron density and n_i is the ion density.

In order to solve the Vlasov equation we use a method of separation of time scales [22] between the characteristic time of variation of the potential and the transit time of an electron into this potential. This time scale separation is a consequence of the smallness of the mass ratio m_e/m_i. It allows us to build an adiabatic motion invariant so that we can reconstruct the

*patrick.mora@cpht.polytechnique.fr

distribution function of the electrons at any time and at any position by following the time evolution of the total energy of a limited number of electrons (typically less than 100). The time step Δt is chosen to satisfy the plasma stability and in most cases is such that $\Delta t = 0.2/\max(\omega_{\rm pih},\omega_{\rm pic})$, where $\omega_{\rm pih} = (Zn_{h0}e^2/m_i\epsilon_0)^{1/2}$ and $\omega_{\rm pic} = (Zn_{c0}e^2/m_i\epsilon_0)^{1/2}$.

We consider the expansion into a vacuum of a plasma slab with initial width L. The initial ion density is defined as $n_i = n_0$ for $|x| \leqslant L/2$ and $n_i = 0$ for $|x| > L/2$, where x is the direction normal to the target ($x = 0$ corresponds to the center of the foil). As the expansion is symmetric with respect to the target center, one may restrict the calculation to the positive part of the plasma slab.

The electron population is composed of a hot component and a cold component corresponding respectively to distribution functions $f_h(x,v,t)$ and $f_c(x,v,t)$ and densities

$$n_{h,c}(x,t) = \int f_{h,c}(x,v,t)dv, \tag{4}$$

with $f_e = f_h + f_c$ and $n_e = n_h + n_c$. Initially these two components are represented by Maxwellian distribution functions f_{h0} and f_{c0} with

$$f_{h0}(x,v) = n_{h0}\left(\frac{m_e}{2\pi k_B T_{h0}}\right)^{1/2}\exp\left(-\frac{\mathcal{E}}{k_B T_{h0}}\right), \tag{5}$$

where k_B is the Boltzmann constant, T_{h0} is the initial hot temperature, and $\mathcal{E}$ is the total energy of the electron $\mathcal{E} = \frac{1}{2}m_e v^2 - e\Phi$. A similar expression can be written for $f_{c0}(x,v)$, with n_{h0} replaced by n_{c0} and T_{h0} replaced by T_{c0}, where T_{c0} is the initial cold temperature. The densities n_{h0} and n_{c0} verify $n_{h0} + n_{c0} = Zn_0$ and the electrostatic potential adjusts itself so that Eq. (3) is verified everywhere and $\partial\Phi/\partial x \to 0$ when $|x| \to \infty$ (which ensures global neutrality).

Though the distribution functions do not remain Maxwellian during the expansion, it is still possible to define a hot and a cold electron temperature at any time and any position, with

$$k_B T_h(x,t) = \frac{m_e\int v^2 f_h(x,v,t)dv}{n_h(x,t)}, \tag{6}$$

and a similar expression for $T_c(x,t)$, with f_h and n_h replaced by f_c and n_c. One can also define a global temperature $T_h(t)$ by averaging $T_h(x,t)$ over the simulation box,

$$T_h(t) = \frac{\int n_h(x,t)T_h(x,t)dx}{\int n_h(x,t)dx}, \tag{7}$$

with a similar expression for the global temperature $T_c(t)$, with n_h and T_h replaced by n_c and T_c.

For convenience we define the two dimensionless parameters

$$y = n_{h0}/n_{c0}, \quad \alpha = T_{h0}/T_{c0}. \tag{8}$$

In all our simulations the ratio of the hot to cold electron temperature satisfies $\alpha \gg 1$.

The initial ion acoustic velocity is given by

$$c_{s0} = c_{sh0}\sqrt{\frac{1+y}{\alpha+y}}, \tag{9}$$

where c_{sh0} is the ion acoustic velocity, which would be due to hot electrons only,

$$c_{sh0} = \sqrt{\frac{Zk_B T_{h0}}{m_i}}. \tag{10}$$

We define the characteristic time

$$\tau = L/c_{sh0}, \tag{11}$$

which is approximately twice the disassembly time of the foil in the absence of cold electrons [20,21,23]. Unless specified otherwise, the plasma slab has an initial width $L/2\lambda_{Dh0} = 20$, where $\lambda_{Dh0} = (\epsilon_0 k_B T_{h0}/n_{h0}e^2)^{1/2}$.

B. Semi-infinite case

It is instructive to first recall the main results corresponding to the semi-infinite case [15,19]. Figure 1 illustrates the profile of the electrostatic potential obtained in the quasineutral limit for a semi-infinite plasma, with $\alpha = 10^2$ and $y = 10^{-2}$. The following regions are identified: the unperturbed plasma on the left of the rarefaction wave situated in A, an expansion dominated by cold electrons between A and B, the rarefaction shock joining B and E, a plateau between E and F, and an expansion dominated by hot electrons on the right of F. The dashed line corresponds to the mathematical multivalued solution obtained by solving ξ as a function of ϕ (see Ref. [19] for details).

In the limit $\alpha \gg 1$, the expressions of the density ratios corresponding to the positions B and D are given by [19]

$$y_B \approx \frac{2.22}{\sqrt{\alpha}} + \frac{4.57}{\alpha}, \tag{12}$$

$$y_D \approx \frac{\alpha^2}{2} - 3\alpha \tag{13}$$

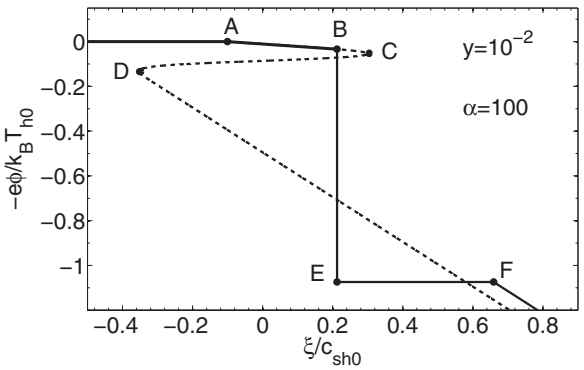

FIG. 1. Semi-infinite case ($L \to \infty$). Electric potential ϕ as a function of the self-similar parameter $\xi = (|x| - L/2)/t$, calculated in the quasineutral limit for $\alpha = 10^2$ and $y = 10^{-2}$. Here $\xi = 0$ corresponds to the edge of the foil at $t = 0$. The curve shows a rarefaction shock and a plateau on the downstream side of the shock. Also shown (as a dashed line) is the mathematical multivalued solution obtained by solving ξ as a function of ϕ. (This figure is adapted from Fig. 2 of Ref. [19].)

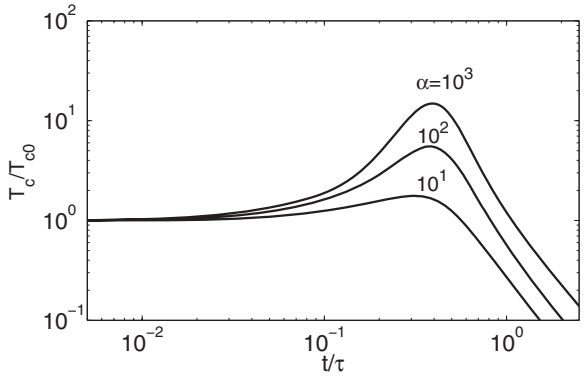

FIG. 2. Cold electron mean temperature as a function of time for $y = 10^4$, $L/2\lambda_{Dh0} = 20$, and $\alpha = 10$, 10^2, and 10^3.

and the position of the rarefaction shock ξ_B is given (for $y_B > y$) by

$$\xi_B \approx \left[\ln\left(\frac{y_B}{y}\right) + \frac{y}{2} - y_B - 1\right]\frac{c_{sh0}}{\sqrt{\alpha}}. \tag{14}$$

Depending on y, one may in fact distinguish three main regimes [19].

(i) When $y_B > y$, the structure of the flow is as depicted in Fig. 1. The rarefaction wave moves towards the plasma at the ion acoustic velocity $c_{s0} \approx c_{sc0} = (Zk_BT_{c0}/m_i)^{1/2}$. The rarefaction shock moves towards either the vacuum when $\xi_B > 0$ or the plasma when $\xi_B < 0$. The two subregimes' frontier is given by setting $\xi_B = 0$ in Eq. (14), i.e., $y \approx 0.82/\sqrt{\alpha}$.

(ii) When $y_D > y > y_B$, the region of the flow dominated by cold electrons disappears and the unperturbed plasma is directly connected to the rarefaction shock. In addition, the shock propagates inside the plasma at a supersonic velocity, intermediate between c_{s0} and c_{sh0}.

(iii) When $y > y_D$, the flow is entirely dominated by hot electrons and there is no more rarefaction shock. The rarefaction wave moves towards the plasma at the ion acoustic velocity $c_{s0} \approx c_{sh0}$. The cold electrons behave as test particles.

Regime (i) is relevant for most experiments where the hot electrons are a minor fraction of the total number of electrons. However, the two other regimes show interesting features, which we will first present in the following section.

III. EXPANSION DOMINATED BY HOT ELECTRONS

In this section we consider the case where the expansion is dominated by hot electrons, corresponding to regime (iii) of the preceding section or to regime (ii) in the case where the rarefaction shock amplitude is negligible. As a first approximation, the thin-foil expansion is driven by hot electrons only and is described in Ref. [21]. It can be separated into two phases. In the first phase ($t \lesssim 0.4\,\tau$), a rarefaction wave progresses towards the center of the foil. For time $t \gtrsim 0.4\tau$ the whole foil disassembles.

The cold electrons can be considered as test particles as they do not modify significantly the characteristics of the expansion. Figure 2 shows the time evolution of the global cold temperature $T_c(t)$ for $y = 10^4$ and for different values of α ranging from 10 to 10^3.

We observe a heating of the cold electron population during the first phase. The cold temperature increases until a time that corresponds approximately to the arrival of the rarefaction wave at the center of the target, which is $t_r/\tau \approx 0.4$. During this first phase of the expansion, the hot electrons supply both the expanding ions and the cold electrons with energy. Beyond this time, the cold electrons start cooling down and both hot electrons and cold electrons transfer their energy to the ions. As expected, this heating is more efficient with higher values of the temperature ratio α. The heating is as large as a factor of 15 for $\alpha = 10^3$ when the rarefaction wave reaches the center of the foil.

To interpret these results, we present simple analytic considerations. Let us first consider the initial phase of the expansion $\lambda_{Dh0} \ll c_{sh0}t \ll L$. A self-similar expansion is established on both sides of the foil, with

$$e\Phi(x,t) \simeq -k_BT_{h0}[1 + (|x| - L/2)/c_{sh0}t]. \tag{15}$$

One can use the results of Refs. [20,21,24] to calculate the energy variation rate of a slow electron due to the energy exchange in the time-varying electrostatic fields on both sides of the foil,

$$d\mathcal{E}/dt \simeq 4\mathcal{E}/\tau, \tag{16}$$

where $\mathcal{E} = \frac{1}{2}m_ev^2$ ($\mathcal{E} \ll k_BT_{h0}$). To first order in t, one can express the energy $\mathcal{E}(t)$ of a slow electron as a function of its initial energy $\mathcal{E}_0$ and invert to obtain

$$\mathcal{E}_0 \simeq (1 - 4\,t/\tau)\mathcal{E}(t). \tag{17}$$

Now using the fact that the value of the distribution function is conserved along each electron trajectory, one gets in the inner part of the foil ($|x| + c_{sh0}t < L/2$)

$$f_c(x,v,t) \simeq \left(1 + \frac{2m_ev^2}{k_BT_{c0}}\frac{t}{\tau}\right) f_{c0}(v) \tag{18}$$

and

$$n_c(t) \simeq n_{c0}(1 + 2\,t/\tau), \tag{19}$$

$$T_c(t) \simeq T_{c0}(1 + 4\,t/\tau). \tag{20}$$

These two equations show that the cold electrons are adiabatically compressed by the electrostatic potential, with $T_c \propto n_c^{\gamma-1}$ and $\gamma = 3$. One can go a little bit further in the analysis by noticing that the cold electrons are in fact confined by the electrostatic potential to the region that has not been attained by the rarefaction wave. The width of this region is approximately given by

$$L_c(t) \simeq L - 2c_{sh0}t = L(1 - 2\,t/\tau). \tag{21}$$

The cold electron density goes up as $n_c(t) \simeq n_{c0}L/L_c$ and the cold electron temperature as $T_c(t) \simeq T_{c0}(L/L_c)^2$, i.e.,

$$T_c(t) \simeq \frac{T_{c0}}{(1 - 2\,t/\tau)^2}. \tag{22}$$

The first-order expansion of Eq. (22) in power of t/τ coincides with Eq. (20). However, it is clear from Fig. 3, which shows the numerical result and the two analytical expressions (20) and (22), that Eq. (22) gives a better account of the temperature behavior for intermediate time.

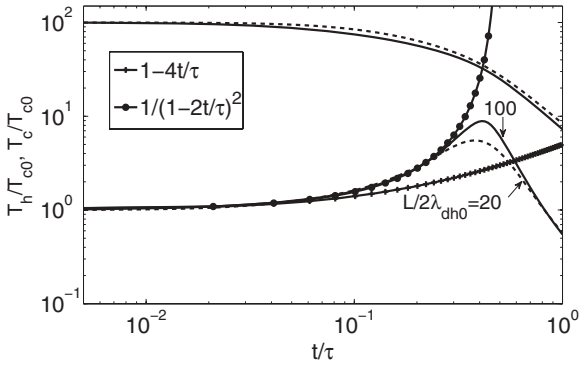

FIG. 3. Temporal evolution of the cold and hot electron mean temperatures for $\alpha = 10^2$ and $y = 10^4$. The initial widths of the plasma are $L/2\lambda_{Dh0} = 20$ (dashed lines) and $L/2\lambda_{Dh0} = 100$ (solid lines). The plus sign line is the result of Eq. (20), while the black circle line corresponds to Eq. (22).

The above analysis becomes invalid when the rarefaction wave reaches the center of the foil. To estimate the maximum temperature attained by the cold electrons, we assume that when the rarefaction wave reaches the center of the foil the electrostatic potential is still given by Eq. (15) with $t = \tau/2$ and T_{h0} replaced by $T_h(t = \tau/2) \approx T_{h0}/3$, i.e.,

$$e\Phi(x,t = \tau/2) \simeq -\frac{2}{3}k_B T_{h0}\frac{|x|}{L}, \tag{23}$$

and that the cold electrons extension $L_{c,\min}$ is such that $e|\Phi(L_{c,\min}/2)| \approx k_B T_{c,\max}$, with again $T_{c,\max}(t) \simeq T_{c0}(L/L_c)^2$, so that

$$k_B T_{c,\max} \approx k_B T_c(\alpha/3)^{2/3}, \tag{24}$$

in good agreement with the numerical results for $L/2\lambda_{Dh0} \geqslant 100$.

Note here that the temperature increase we observe in Fig. 3 is not specific to the kinetic model, as it is also seen, though with a smaller amplitude, with a hybrid code, where the hot and cold distribution functions are forced to stay Maxwellian at any time [23]. To illustrate this assertion, we plot in Fig. 4 the cold electron mean temperature versus time obtained with the present kinetic code and with the hybrid code of Ref. [23], for $\alpha = 10^2$, $y = 10^4$, and $L/2\lambda_{Dh0} = 20$.

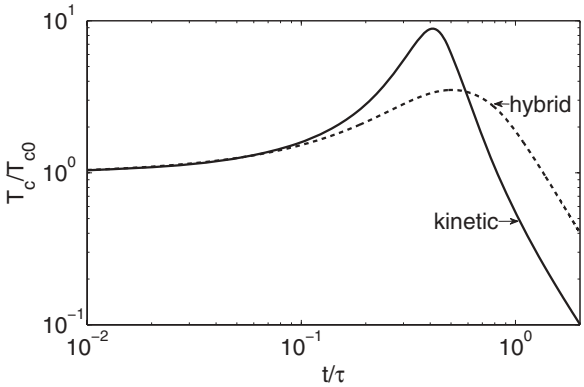

FIG. 4. Temporal evolution of the cold electron mean temperature for $\alpha = 10^2$, $y = 10^4$, and $L/2\lambda_{Dh0} = 20$ for the kinetic (solid line) and hybrid (dashed line) models.

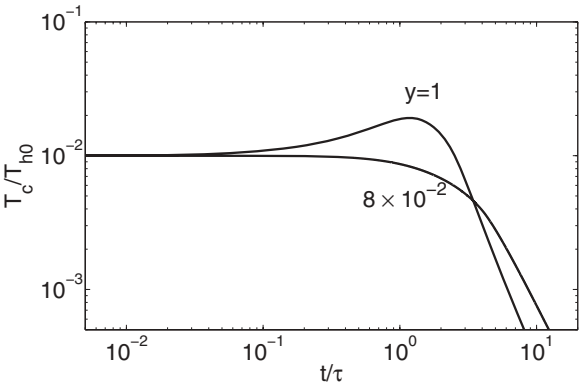

FIG. 5. Temporal evolution of the cold electron mean temperature for intermediate values of y ($y = 1$ and 8×10^{-2}) with $\alpha = 10^2$ and $L/2\lambda_{Dh0} = 20$.

IV. INTERMEDIATE REGIME

Figure 5 illustrates the time variation of the cold electron mean temperature for $y = 1$ and 8×10^{-2}. As can be seen, the amplification process of the cold electron temperature is reduced for $y = 1$ and vanishes for $y = 8 \times 10^{-2}$. This can be understood easily. When $y = 1$, the rarefaction shock propagates inside the plasma at a velocity that is larger than c_{s0} but smaller than c_{sh0} and the corresponding potential jump compresses and adiabatically heats the cold electron component, in a way similar to what was described in the preceding section.

When $y = 8 \times 10^{-2}$ the rarefaction shock almost stays at the edge of the plasma as $\xi_B \approx 0$ according to Eq. (14) and no cold electron compression and heating occur. Eventually, as the hot electron temperature and density go down due to the plasma expansion, the instantaneous value of ξ_B increases with time, leading to a decrease of the cold electron density and temperature.

V. REGIME DOMINATED BY COLD ELECTRONS

The studies of the preceding sections were somewhat academic in the sense that the values of the initial ratios of the densities y in the undisturbed plasma were quite different from those that occur in the interaction of an ultrahigh intense

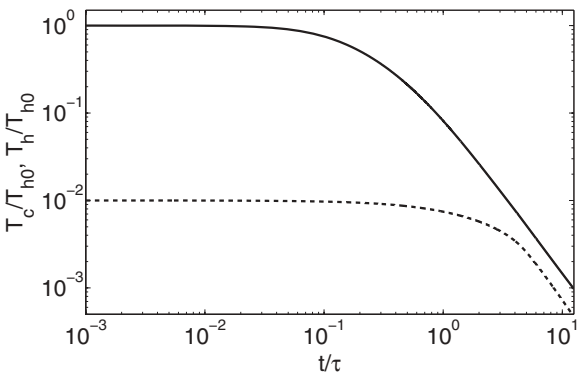

FIG. 6. Temporal evolution of the hot (solid line) and cold (dashed line) electron mean temperature for $y = 10^{-2}$, $\alpha = 10^2$, and $L/2\lambda_{Dh0} = 20$.

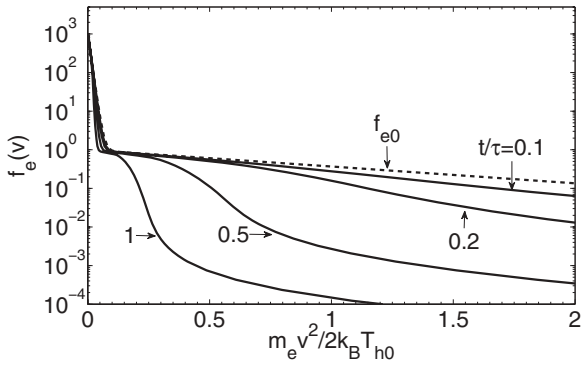

FIG. 7. Electron distribution function for a plasma slab with initial parameters $\alpha = 10^2$, $y = 10^{-2}$, and $L/2\lambda_{Dh0} = 20$ and at different times $t/\tau = 0, 0.1, 0.2, 0.5$, and 1. The distribution function is taken at the center of the plasma slab $x = 0$ and is normalized to f_{h0}.

laser with solid targets. In this section we propose to consider more realistic values of the initial densities ratios, i.e., $y \ll 1$.

A. Global cooling of electrons

In Fig. 6 we show the time variation of the hot and the cold electron mean temperature for $y = 10^{-2}$, $\alpha = 10^2$, and $L/2\lambda_{Dh0} = 20$. Both the cold and hot electrons cool down. However, the hot electrons cool down earlier than cold electrons. The characteristic cooling time is τ for hot electrons and $\tau\sqrt{\alpha}$ for cold electrons (the rarefaction wave velocity is approximatively $c_{s0} \approx c_{sh0}/\sqrt{\alpha}$). As the temperature behaves as t^{-2} for large times, the two curves eventually tend to be quite close.

Let us now discuss the evolution of the electron distribution function for the case of Fig. 6. Figure 7 shows the electron distribution function for a plasma slab with initial parameters $L/2\lambda_{Dh0} = 20$, $y = 10^{-2}$ and $\alpha = 10^2$ at different times of the expansion. The electron distribution function is taken at the center of the plasma slab $x = 0$. For times $t \geqslant \tau$, the structure of the distribution function that is initially a bi-Maxwellian function moves towards a two top-hat structure.

As demonstrated in Ref. [21] in the case of a single temperature distribution function, the distortion of the electron distribution function initially leads to an increase of the

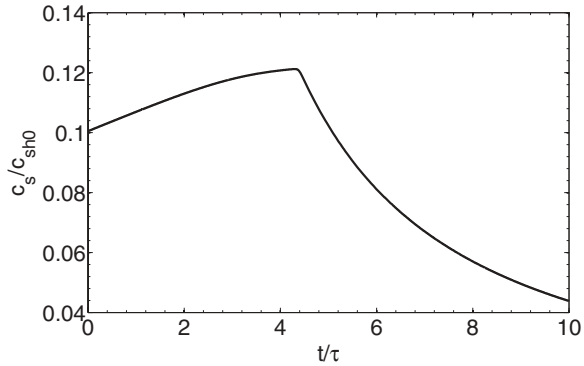

FIG. 8. Ion acoustic velocity at the center of the foil as a function of time for $\alpha = 10^2$, $y = 10^{-2}$, and $L/2\lambda_{Dh0} = 20$.

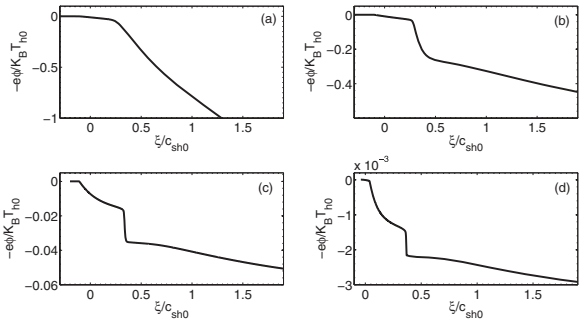

FIG. 9. Electric potential ϕ as a function of $\xi = (|x| - L/2)/t$ at times (a) $\omega_{\rm pih}t = 4$, (b) $\omega_{\rm pih}t = 20$, (c) $\omega_{\rm pih}t = 100$, and (d) $\omega_{\rm pih}t = 500$. The plasma initial parameters are $\alpha = 10^2$, $y = 10^{-2}$, and $L/2\lambda_{Dh0} = 20$.

ion acoustic velocity and of the rarefaction wave. Once the rarefaction wave has reached the center of the foil, the global cooling of the electrons leads to a decrease of the ion acoustic velocity. This behavior is illustrated in Fig. 8 for the case of Figs. 6 and 7.

B. Spatial profiles

Figure 9 shows the electric potential as function of $\xi = (|x| - L/2)/t$ for $y = 10^{-2}$ and at times $\omega_{\rm pih}t = 4, \omega_{\rm pih}t = 20$, $\omega_{\rm pih}t = 100$, and $\omega_{\rm pih}t = 500$. One observes that the structure of the rarefaction shock is still apparent at late time of the expansion, but the value of the potential jump is declining in time. For instance, at time $\omega_{\rm pih}t = 500$, the value of the jump of the rarefaction is reduced by more than three orders of magnitude compared to its value for a semi-infinite case. In comparison with the results obtained in the semi-infinite case, we also remark that the expansion tends to reduce the length of the plateau (compare Fig. 9 with Fig. 12 of Ref. [19]).

Figure 10 shows the electric field as a function of ξ at times $\omega_{\rm pih}t = 20$ and 100. The electric field is normalized to $E_0 = (n_{h0}k_B T_{h0}/\epsilon_0)^{1/2}$. We observe two different peaks. The first one corresponds to the rarefaction shock while the second one is related to the ion front as shown in Refs. [19–21]. The inset

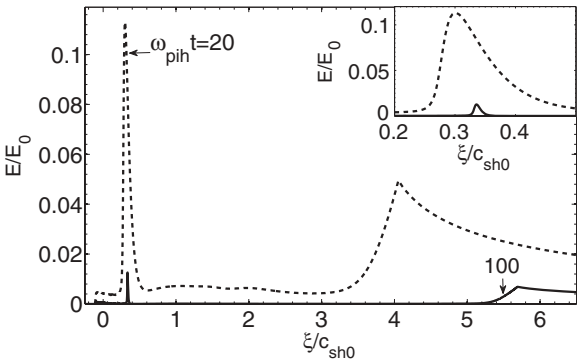

FIG. 10. Electric field as a function of $\xi = (|x| - L/2)/t$ at times $\omega_{\rm pih}t = 20$ and $\omega_{\rm pih}t = 100$. The plasma slab initial parameters are $\alpha = 10^2$ and $y = 10^{-2}$. The inset is a zoom around the rarefaction shock position. The electric field is normalized to $E_0 = (n_{h0}k_B T_{h0}/\epsilon_0)^{1/2}$.

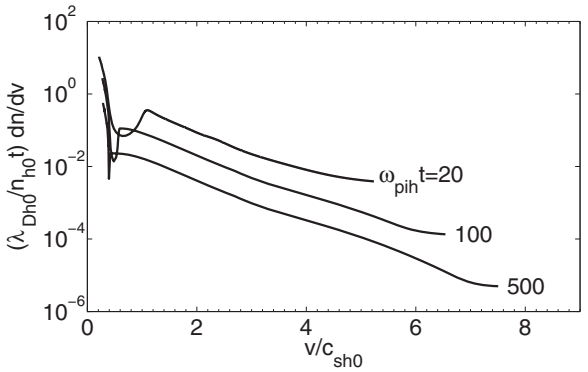

FIG. 11. Normalized ion velocity spectrum versus velocity v for a plasma foil with the initial parameters $\alpha = 10^2$ and $y = 10^{-2}$ and at times $\omega_{pih}t = 20$, 100, and 500.

of Fig. 10 represents a zoom of the peak of the electric field in the rarefaction shock. Conversely to the semi-infinite case, the peak associated with the rarefaction shock is not steady in time, but moves slowly towards the vacuum. One also notes that the amplitude of the electric field at the ion front decreases faster than $2E_0/\omega_{pih}t$, which is the value corresponding to the semi-infinite case.

C. Ion velocity distribution

The ion velocity distribution is shown in Fig. 11 for $y = 10^{-2}$, $\alpha = 10^2$, and at times $\omega_{pih}t = 20$, 100, and 500. We observe that the dip in the ion velocity spectra, which increases with time in the semi-infinite case [19], tends to decrease and to narrow here. We also see that the Dirac δ function corresponding to the density and velocity plateau of the self-similar solution shown in Ref. [19] seems to completely disappear here.

VI. CONCLUSION

The expansion of a plasma foil composed of hot electrons and cold electrons with an initially bi-Maxwellian electron distribution function has been studied with a one-dimensional kinetic code. Attention has been focused on the energy exchange between electrons and ions and two mains cases have been identified.

When the ratio of the hot to cold electron densities y is large enough, typically for $y \geqslant 10^{-1}$ when $\alpha = 10^2$, we demonstrate that the cold electron mean temperature first increases at the expense of hot electrons, due to an adiabatic compression by the electric potential. The cold electron heating takes place during the first phase of the expansion, i.e., while the rarefaction wave moves towards the center of the foil. When the rarefaction wave arrives at the center of the foil, the cold electrons start cooling.

In contrast, when $y \ll 1$, as in most experiments, we observe a global cooling of both cold and hot electrons. However, the hot electron temperature decreases initially faster than the cold electron temperature, thus reducing the temperature ratio.

As a result of the electron cooling, the amplitude of the shock and the length of the plateau are deeply reduced. In addition, the dip and the peak observed in the velocity spectrum in the semi-infinite case are almost absent in the case of a thin foil.

Finally, it is important to note that this paper is restricted to a purely one-dimensional expansion. However, due to the anisotropy of the electron distribution function, electromagnetic (Weibel) instabilities are expected to develop during the expansion of the plasma foil if the electron thermal velocity is not too small compared with the light velocity. The anisotropy might exist initially (when the longitudinal electron temperature, i.e., perpendicular to the foil surface, is larger than the transverse electron temperature, i.e., along the foil surface) or appear as a result of the expansion itself (when the longitudinal temperature becomes lower than the transverse temperature, due to the cooling that affects only the longitudinal temperature), as described in Ref. [25]. Though the cold electrons tend to have a stabilizing effect in the early time of the expansion, their role appears less important at long time. The magnetic field due to the instability, by exchanging energy between the longitudinal and the transverse dimensions as binary collisions would do in a collisional plasma, contributes to suppress the anisotropy and thus the source of the instability that usually saturates. It thus gives the expansion a three-dimensional character, with a characteristic adiabatic parameter $\gamma = 5/3$ instead of $\gamma = 3$, eventually giving a time dependence of the temperature $T \propto t^{-2/3}$ at late times rather than $T \propto t^{-2}$. Further details would need a more precise analysis, which is beyond the scope of the present paper.

[1] J. Fuchs *et al.*, Nat. Phys. **2**, 48 (2006).
[2] T. E. Cowan *et al.*, Phys. Rev. Lett. **92**, 204801 (2004).
[3] P. K. Patel, A. J. Mackinnon, M. H. Key, T. E. Cowan, M. E. Foord, M. Allen, D. F. Price, H. Ruhl, P. T. Springer, and R. Stephens, Phys. Rev. Lett. **91**, 125004 (2003).
[4] R. A. Snavely *et al.*, Phys. Rev. Lett. **85**, 2945 (2000).
[5] M. Tabak *et al.*, Phys. Plasmas **1**, 1626 (1994).
[6] S. V. Bulanov *et al.*, Phys. Lett. A **299**, 240 (2002).
[7] M. I. K. Santala *et al.*, Appl. Phys. Lett. **78**, 19 (2001).
[8] A. V. Gurevich, L. V. Pariiskaya, and L. P. Pitaevskii, Zh. Eksp. Teor. Fiz. **49**, 647 (1965) [Sov. Phys. JETP **22**, 449 (1966)].
[9] J. E. Crow, P. L. Auer, and J. E. Allen, J. Plasma Phys. **14**, 65 (1975).
[10] V. F. Kovalev, V. Yu. Bychenkov, and V. T. Tikhonchuk, Zh. Eksp. Teor. Fiz. **122**, 264 (2002) [Sov. Phys. JETP **95**, 226 (2002)].
[11] P. Mora, Phys. Rev. Lett. **90**, 185002 (2003).
[12] V. Y. Bychenkov *et al.*, Phys. Plasmas **11**, 3242 (2004).
[13] P. Mora, Phys. Rev. E **72**, 056401 (2005).
[14] R. L. Morse and C. W. Nielson, Phys. Fluids **16**, 909 (1973).
[15] B. Bezzerides, D. W. Forslund, and E. L. Lindman, Phys. Fluids **21**, 2179 (1978).

[16] L. M. Wickens, J. E. Allen, and P. T. Rumsby, Phys. Rev. Lett. **41**, 243 (1978).
[17] M. A. True, J. R. Albritton, and E. A. Williams, Phys. Fluids **24**, 1885 (1981).
[18] M. Passoni, V. T. Tikhonchuk, M. Lontano, and V. Y. Bychenkov, Phys. Rev. E **69**, 026411 (2004).
[19] A. Diaw and P. Mora, Phys. Rev. E **84**, 036402 (2011).
[20] T. Grismayer, P. Mora, J. C. Adam, and A. Héron, Phys. Rev. E **77**, 066407 (2008).
[21] P. Mora and T. Grismayer, Phys. Rev. Lett. **102**, 145001 (2009).
[22] L. D. Landau and E. M. Lifshitz, *Mechanics*, 3rd ed. (Butterworth-Heinemann, Oxford, 1976).
[23] P. Mora, Phys. Plasmas **12**, 112102 (2005).
[24] P. Mora and R. Pellat, Phys. Fluids **22**, 2300 (1979).
[25] C. Thaury, P. Mora, A. Heron, J. C. Adam, and T. M. Antonsen, Phys. Rev. E **82**, 026408 (2010).